

# Ultra-reducing conditions in average mantle peridotites and in podiform chromitites: a thermodynamic model for moissanite (SiC) formation

Anastasia Golubkova<sup>1</sup> · Max W. Schmidt<sup>1</sup> · James A. D. Connolly<sup>1</sup>

Received: 21 December 2014 / Accepted: 21 March 2016  
© Springer-Verlag Berlin Heidelberg 2016

**Abstract** Natural moissanite (SiC) is reported from mantle-derived samples ranging from lithospheric mantle keel diamonds to serpentinites to podiform chromitites in ophiolites related to suprasubduction zone settings (Luobusa, Dongqiao, Semail, and Ray-Iz). To simulate ultra-reducing conditions and the formation of moissanite, we compiled thermodynamic data for alloys (Fe–Si–C and Fe–Cr), carbides (Fe<sub>3</sub>C, Fe<sub>7</sub>C<sub>3</sub>, SiC), and Fe-silicides; these data were augmented by commonly used thermodynamic data for silicates and oxides. Computed phase diagram sections then constrain the  $P$ – $T$ – $fO_2$  conditions of SiC stability in the upper mantle. Our results demonstrate that: Moissanite only occurs at oxygen fugacities 6.5–7.5 log units below the iron–wustite buffer; moissanite and chromite cannot stably coexist; increasing pressure does not lead to the stability of this mineral pair; and silicates that coexist with moissanite have  $X_{Mg} > 0.99$ . At upper mantle conditions, chromite reduces to Fe–Cr alloy at  $fO_2$  values 3.7–5.3 log units above the moissanite-olivine-(ortho)pyroxene-carbon (graphite or diamond) buffer (MOOC). The occurrence of

SiC in chromitites and the absence of domains with almost Fe-free silicates suggest that ultra-reducing conditions allowing for SiC are confined to grain scale microenvironments. In contrast to previous ultra-high-pressure and/or temperature hypotheses for SiC origin, we postulate a low to moderate temperature mechanism, which operates via ultra-reducing fluids. In this model, graphite-/diamond-saturated moderately reducing fluids evolve in chemical isolation from the bulk rock to ultra-reducing methane-dominated fluids by sequestering H<sub>2</sub>O into hydrous phases (serpentine, brucite, phase A). Carbon isotope compositions of moissanite are consistent with an origin of such fluids from sediments originally rich in organic compounds. Findings of SiC within rocks mostly comprised by hydrous phases (serpentine + brucite) support this model. Both the hydrous phases and the limited diffusive equilibration of SiC with most minerals in the rocks indicate temperatures below 700–800 °C. Moissanite from mantle environments is hence a mineral that does not inform on pressure but on a low to moderate temperature environment involving ultra-reduced fluids. Any mineral in equilibrium with SiC could only contain traces of Fe<sup>2+</sup> or Cr<sup>3+</sup>.

Communicated by Chris Ballhaus.

**Electronic supplementary material** The online version of this article (doi:10.1007/s00410-016-1253-9) contains supplementary material, which is available to authorized users.

✉ Max W. Schmidt  
max.schmidt@erdw.ethz.ch

Anastasia Golubkova  
agolubkova@munichre.com

James A. D. Connolly  
james.connolly@erdw.ethz.ch

<sup>1</sup> Institute of Geochemistry and Petrology, ETH Zurich, Clausiusstrasse 25, 8092 Zurich, Switzerland

**Keywords** Moissanite · SiC · Ultra-reducing · Thermodynamic database · Iron–silicon–carbon alloys · Iron–chrome alloys · Iron silicides and carbides · COH fluids

## Introduction

The mantle redox state is a key factor controlling the initiation of melting in the mantle as both carbonate-bearing or metal + C-bearing mantle have distinctively lower solidi than peridotites composed of silicates + oxides + graphite/

diamond (Dasgupta and Hirschmann 2010; Rohrbach et al. 2014). According to models based on mantle-derived rocks and high-pressure experiments, the Earth's mantle becomes progressively more reduced with increasing depth (Frost and McCammon 2008). Estimates for ambient oxygen fugacity ( $fO_2$ ) values of the deeper mantle are mainly based on xenoliths from sub-cratonic regions and are thought to cover a range from near the fayalite–magnetite–quartz equilibrium ( $\Delta\log fO_2[\text{FMQ}] \approx \pm 2$ ) at relatively shallow depths (<60 km) to the iron–wustite buffer (IW,  $\Delta\log fO_2[\text{FMQ}] \approx -5$ ) at  $\geq 250$  km. Oxygen fugacities close to the IW equilibrium result from precipitation of Fe–Ni alloy which, in turn, is a consequence of  $\text{Fe}^{2+}$  disproportionation and  $\text{Fe}^{3+}$  substitution into high-pressure mantle silicates (mainly majorite, wadsleyite, and perovskite). If the mantle is characterized by a constant Fe:O ratio on a global scale, then the amount of alloy precipitated within the deeper parts of the upper mantle is 0.1–0.2 wt% (Frost and McCammon 2008). In metal-bearing mantle, carbon should be present in its reduced forms, either as diamond/graphite, iron carbides, or as Fe–C melt (Rohrbach et al. 2014).

Although there is a general decrease of  $fO_2$  in the mantle with depth (Frost and McCammon 2008), some mantle-derived samples indicate that local redox conditions may deviate from this trend: The occurrence of carbonate-bearing fluid inclusions in diamonds (e.g., Klein-BenDavid et al. 2009; Kopylova et al. 2010; Zedgenizov et al. 2009) points to a local increase in  $fO_2$  values to the carbon (diamond/graphite)–CO/CO<sub>2</sub> (CCO) buffer at  $P > 5$  GPa. On the other hand, some diamonds contain mineral inclusions of SiC (Gorshkov et al. 1997; Leung 1990; Moore and Gurney 1989; Moore et al. 1986), which stability requires far more reducing conditions than the IW buffer. End-member phase equilibria calculations by Mathez et al. (1995) and Ulmer et al. (1998) have shown that moissanite requires a  $\Delta\log fO_2[\text{IW}]$  of  $-6$  to  $-5$ . Schmidt et al. (2014) have performed experiments and expanded such calculations to include solid solutions arriving at the conclusion that oxygen fugacities 6.5–5 log units lower than the iron–wustite buffer are required for SiC stability.

Moissanite is reported from mantle rocks or samples that formed at different depths. SiC inclusions in diamonds and SiC in kimberlites most likely originate from the sub-cratonic lithosphere. Instead, podiform chromitites have probably formed in relatively shallow mantle environments, most likely in suprasubduction zone settings (Ballhaus 1998; Zhou et al. 1996), and a few of such podiform chromitites in ophiolites contain moissanite (Luobusa, Dongqiao, Semail, and Ray-Iz; Robinson et al. 2004, 2015; Bai et al. 2000; Yamamoto et al. 2009; Liou et al. 2014). SiC grains extracted from heavy mineral concentrates may be accompanied by metals (Fe, Si), metal alloys (Ni–Fe–Cr–C or PGE), intermetallic compounds ( $\text{Fe}_3\text{Si}_7$ ,  $\text{FeSi}_2$ ), and

diamond (Bai et al. 2000; Robinson et al. 2004; Trumbull et al. 2009; Yang et al. 2007). The unusual mineral associations with SiC require extraordinary  $fO_2$  conditions, and the presence of SiC within podiform chromitites has attracted particular attention (e.g., Trumbull et al. 2009) as the host rocks are part of peridotite massifs, posing the question what kind of extraordinary history these peridotites had to endure. As a word of caution, one has to be careful not to automatically accept every reported SiC finding in mineral concentrates as natural, and this topic has been addressed in several studies (e.g., Trumbull et al. 2009, Liou et al. 2014).

Podiform chromitites usually occur within the uppermost mantle of ophiolites. Their temperature of formation (1150–1200 °C), estimated from Fe to Mg exchange equilibria between chromite and silicates, indicates a magmatic origin (Ballhaus et al. 1991; Irvine 1965; Matveev and Ballhaus 2002). Several mechanisms have been proposed: The most popular hypothesis postulates that chromitites crystallize as a result of interaction between H<sub>2</sub>O-bearing mafic melts and ophiolitic peridotites at relatively shallow depths, mafic melts initially forming as a consequence of the infiltration of subduction zone-related fluids (Ballhaus 1998; Zhou et al. 1996). One hypothesis (Matveev and Ballhaus 2002) states that podiform chromitites may result from chromite fractionation into a fluid exsolved during migration of a primitive olivine + chromite-saturated water-rich melt through the uppermost mantle.

All measured moissanites have light carbon isotope compositions with  $\delta^{13}\text{C} = -36$  to  $-18$  ‰, and for the findings where moissanite is associated with diamond, these diamonds are also light in  $\delta^{13}\text{C}$  (Mathez et al. 1995, Trumbull et al. 2009). These isotopic compositions, much lighter than average mantle ( $\delta^{13}\text{C} = -5$  ‰, Deines 2002), need to be considered when developing a model of moissanite formation.

In this study we compute phase diagrams to constrain the  $P$ – $T$ – $fO_2$  conditions of SiC stability in the mantle and to understand whether moissanite can be in equilibrium with chromite. Thermodynamic databases used in geoscience are mostly designed to calculate phase relations of oxides and silicates at redox conditions more oxidizing than IW; therefore, we compile the thermodynamic data for alloys, carbides, and silicides necessary to simulate ultra-reducing conditions. On the basis of our results we formulate a model for the generation of ultra-reduced microenvironments in the mantle in line with the light carbon isotope composition of natural SiC.

## Phase diagram computations

To expand the range of  $fO_2$  values at which mantle phase relations can be calculated, we have compiled

**Table 1** Phases used in calculations with the thermodynamic data sources

Phase abbreviation	Phase	Formula <sup>a</sup>	References
Gph	Graphite	C	Dinsdale (1991)
Diam	Diamond	C	Dinsdale (1991)
Si(met)	Metallic Si	Si	Dinsdale (1991)
Fe <sub>3</sub> C	Cementite	Fe <sub>3</sub> C	Gustafson (1985)
Fe <sub>7</sub> C <sub>3</sub>	Fe <sub>7</sub> C <sub>3</sub>	Fe <sub>7</sub> C <sub>3</sub>	Djurovic et al. (2011)
SiC	Moissanite	SiC	Lacaze and Sundman (1991), Miettinen (1998)
FeSiC(fcc)	fcc Fe–Si–C alloy	Fe <sub>x</sub> Si <sub>1-x</sub> V <sub>y</sub> C <sub>1-y</sub>	Lacaze and Sundman (1991), Miettinen (1998)
FeSiC(bcc)	bcc Fe–Si–C alloy	Fe <sub>x</sub> Si <sub>1-x</sub> V <sub>3y</sub> C <sub>3(1-y)</sub>	Lacaze and Sundman (1991), Miettinen (1998)
FeSi	FeSi	FeSi	Lacaze and Sundman (1991), Miettinen (1998)
FeCr(fcc)	fcc Fe–Cr alloy	Fe <sub>x</sub> Cr <sub>1-x</sub>	Xiong et al. (2011)
FeCr(bcc)	bcc Fe–Cr alloy	Fe <sub>x</sub> Cr <sub>1-x</sub>	Xiong et al. (2011)
σFeCr <sup>b</sup>	sigma Fe–Cr alloy	Fe <sub>10</sub> Cr <sub>4</sub> Fe <sub>w</sub> Cr <sub>16-w</sub> , $w \leq 16$	Hertzman and Sundman (1982)
Ol	Olivine	Mg <sub>2x</sub> Fe <sub>2(1-x)</sub> SiO <sub>4</sub>	Holland and Powell (2011)
Opx	Orthopyroxene	Mg <sub>x(2-y)</sub> Fe <sub>(1-x)(2-y)</sub> Al <sub>2y</sub> Si <sub>2-y</sub> O <sub>6</sub>	Holland and Powell (2011)
Gar	Majoritic garnet	[Fe <sub>x</sub> Ca <sub>y</sub> Mg <sub>(1-x+y+z/3)</sub> ] <sub>3</sub> Al <sub>2-2z</sub> Si <sub>3+z</sub> O <sub>12</sub> , $x + y \leq 1$	Holland and Powell (2011), Stixrude and Lithgow-Bertelloni (2011)
Sp	Spinel	Mg <sub>x</sub> Fe <sub>1-x</sub> Al <sub>y</sub> Cr <sub>2-y</sub> O <sub>4</sub>	Holland and Powell (2011), Oka et al. (1984)
Pc <sup>c</sup>	Magnesio-wustite	Mg <sub>x</sub> Fe <sub>1-x</sub> O	Fabrichnaya (1998), Holland and Powell (2011)

<sup>a</sup> Compositional variables,  $x$ ,  $y$ ,  $z$ , may vary between 0 and 1;  $w \leq 16$

<sup>b</sup> Reference end-member Gibbs free energies and interaction parameters corrected to fit the  $\sigma$  – bcc equilibrium at 773 and 1093 K

<sup>c</sup> Reference Gibbs free energy of wustite was corrected to fit high-pressure experimental data for the IW buffer (Campbell et al. 2009)

thermodynamic data for alloys, carbides (Fe<sub>3</sub>C, Fe<sub>7</sub>C<sub>3</sub>, SiC), and iron silicides (Table 1) and combined these with data for silicates and oxides (Holland and Powell 2011). Isobaric  $T$ – $fO_2$  phase diagram sections were calculated at 1–10 GPa with the Perple\_X free energy minimization program (Connolly 2009). Pressures near 1 GPa correspond to the crust–mantle transition, where podiform chromitites are thought to form (Ballhaus 1998; Zhou et al. 1996). Calculations at 6–10 GPa were done to establish whether a SiC + chromite association becomes stable at greater depths.

For modeling (Figs. 1, 2) we considered phase relations in bulk compositions representing a model mantle and podiform chromitites in MgO–Al<sub>2</sub>O<sub>3</sub>–Fe–Si–Cr–C–O<sub>2</sub>. CaO was added in the calculations at  $P > 5$  GPa to stabilize garnet (Table 2); at lower pressures, it would simply result in cpx. As a benchmark, we used the primitive mantle composition of Palme and O'Neill (2003) with the following modifications. The bulk composition (Table 2) was characterized by  $X_{Mg} = 0.91$ , slightly higher than primitive or depleted mantle ( $X_{Mg} = 0.89$ , Palme and O'Neill 2003; Salters and Stracke 2004). The concentration of carbon in the starting composition was 1000 versus ~100 ppm in primitive mantle (Palme and O'Neill 2003) to ensure excess carbon with respect to Fe alloys and hence saturation in carbides and/or graphite or diamond in our computed phase relations. This carbon content is in the range

of source values of enriched MORB (300–1300 ppm, Dasgupta and Hirschmann 2010; Pineau et al. 2004) and may, e.g., result from mantle metasomatism by carbonate melts or fluids (Rohrbach and Schmidt 2011).

For podiform chromitites, different textural types (massive, disseminated, nodular, and brecciated) are characterized by variable chromite contents of ~25–80 % (Zhou et al. 1996). We consider an average bulk composition with 50 wt% chromite and 50 wt% olivine. The chromite composition was taken from Zhou et al. (1996) and has  $X_{Cr} = 0.76$  (Table 2).

### Thermodynamic data of alloys and intermetallic compounds

The metals and intermetallic compounds considered here have relatively low compressibilities; therefore, the use of the Murnaghan equation of state is legitimate for the pressures of interest  $\leq 10$  GPa. Table 3 provides equation of state parameters for these phases.

Thermodynamic models of alloys were formulated in the Fe–Cr binary and Fe–Si–C ternary, the available data being insufficient to model quaternary Fe–Si–C–Cr alloys. At 1 bar the Fe–Si–C system has been assessed for <5 wt% C and <30 wt% Si (Lacaze and Sundman 1991), a range largely sufficient for this study. Stable phases are fcc and bcc Fe–Si–C alloys, Fe–Si–C liquid, Fe<sub>2</sub>Si, FeSi, graphite,

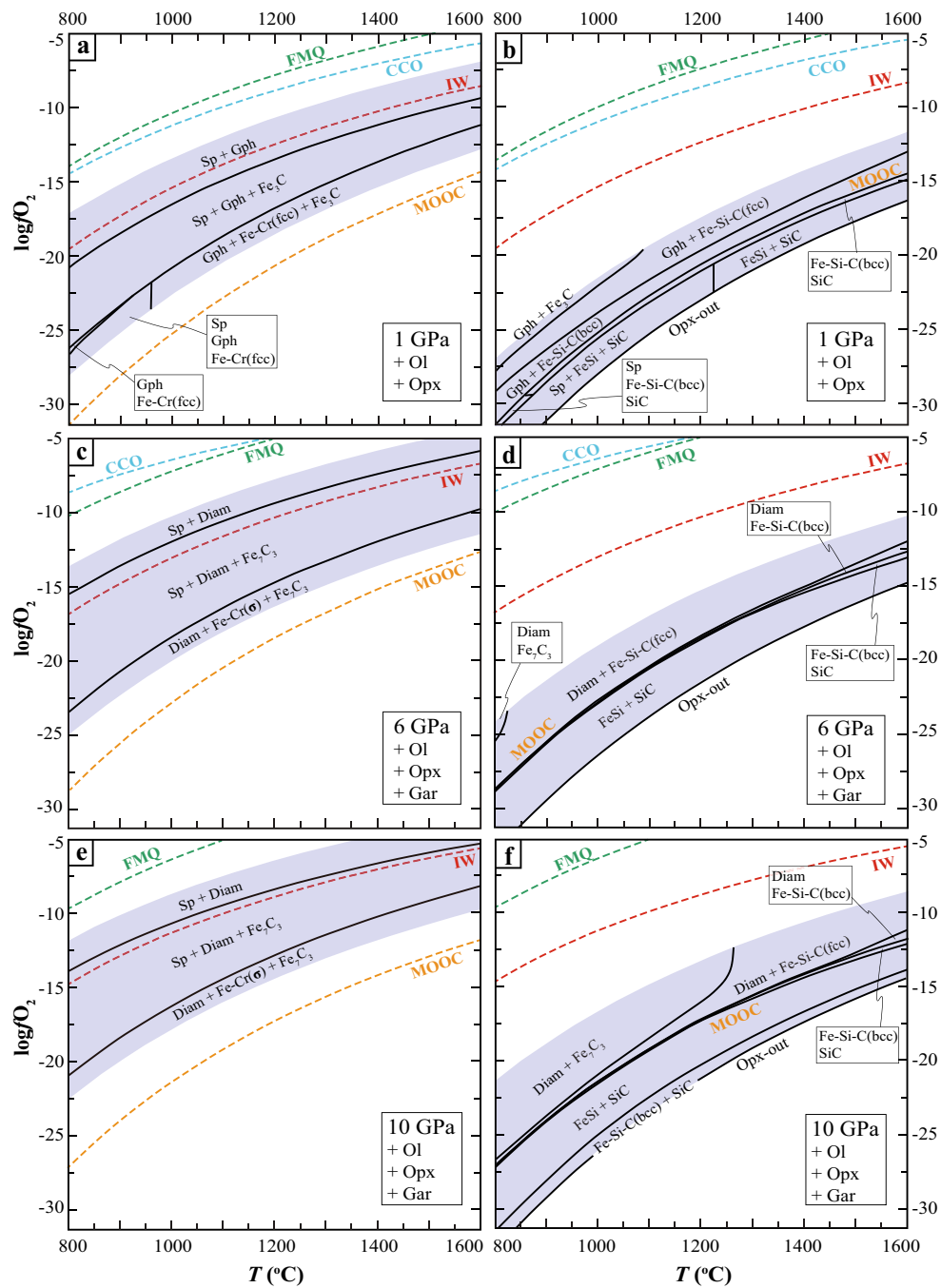


**Fig. 1** Phase relations calculated for a model peridotite composition with 0.1 wt% C (Table 2) at 1, 6, and 10 GPa. Gray regions indicate the range of computation, a restriction caused by the limitations in the extent of available solid solutions: On the *left-hand side*, the bulk has 0.25 wt%  $\text{Cr}_2\text{O}_3$  and the alloys are Fe–Cr in composition, which is a plausible assumption down to oxygen fugacities slightly below the chromite–alloy reaction. On the *right-hand side*, the bulk is Cr-free and the alloys are Fe–Si–C, plausible in the vicinity of SiC stabilization when silicates become reduced to metal and carbides. For details see text. In the Cr-bearing model composition, reduction of chromite terminates spinel stability and leads to the formation of Fe–Cr alloys 3.7–5.3 log units above the SiC-forming reaction. In the Cr-

free model system, a pure MgAl-spinel persists to oxygen fugacities of SiC stability. Reaction (1) defines the moissanite-olivine-orthopyroxene-carbon (graphite or diamond) equilibrium dubbed MOOC, and reference equilibria given as stippled line are calculated for the pure simple systems (CCO, graphite/diamond–CO– $\text{CO}_2$ ; FMQ, fayalite–magnetite–quartz; IW, iron–wustite). At 10 GPa, the CCO buffer locates under the figure label in the upper left corner. Note that at 6 and 10 GPa, garnet is stable across the entire range of calculations. Sp—quaternary  $(\text{Mg}, \text{Fe}^{2+})(\text{Cr}, \text{Al})_2\text{O}_4$  spinel; Diam—diamond; Gph—graphite; Gar—garnet; Ol—olivine; Opx—orthopyroxene; Pc—periclase; Sp—spinel. Fe–Cr( $\sigma$ ) is Fe–Cr alloy in sigma structure, and Fe–Si–C(bcc, fcc) is Fe–Si–C alloy in bcc or fcc structure

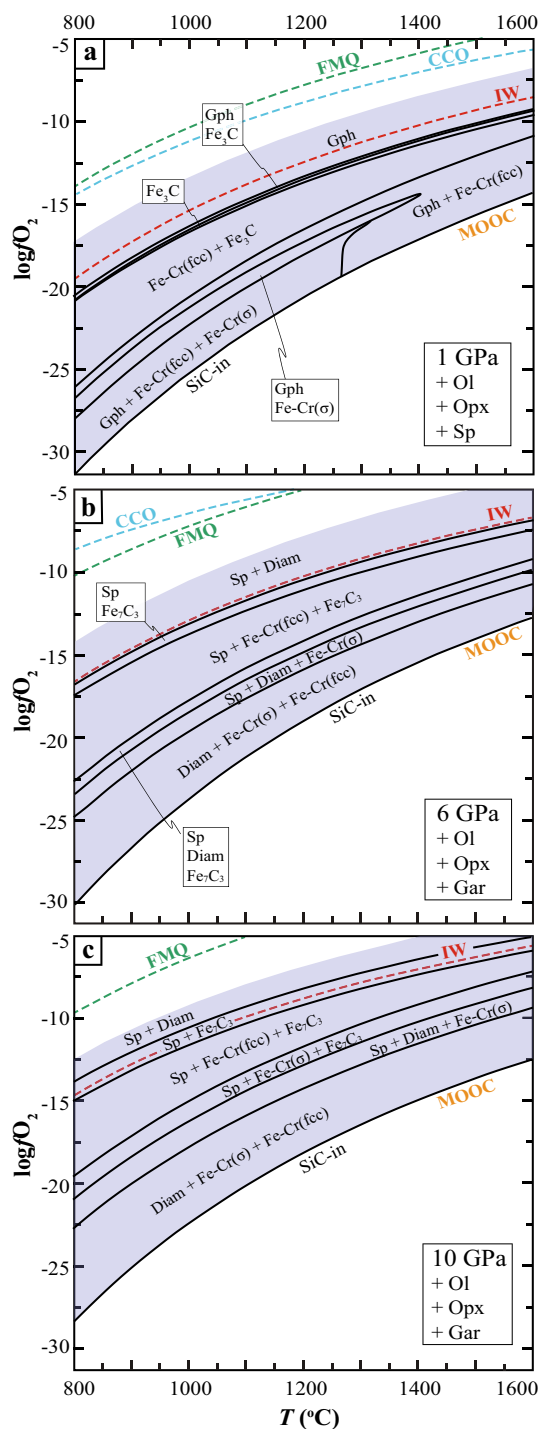


**Fig. 2** Phase relation calculated for a chromitite model composition with 0.1 wt% C (Table 2) at 1, 6, and 10 GPa. Diagrams were computed only in the gray regions at redox conditions more oxidizing than SiC stability. At 1 GPa, quaternary (Mg,Fe<sup>2+</sup>)(Cr,Al)<sub>2</sub>O<sub>4</sub> spinel is stable across the computed range, but becomes MgAl rich with less than a few mol % chromite at the SiC-forming reaction. For phase compositions see Fig. 3, simple buffer reactions and phase abbreviations as in Fig. 1. Note that some stability fields are too tightly clustered to be graphically represented (e.g., the Sp + Diam + Fe<sub>7</sub>C<sub>3</sub> field at 6 GPa)

**Table 2** Bulk compositions (wt%)

	Peridotite	Chromitite
MgO	36.27	27.76
SiO <sub>2</sub>	43.18	26.79
FeO	6.47	11.07
Cr <sub>2</sub> O <sub>3</sub>	0.25	29.35
C	0.10	0.01
Al <sub>2</sub> O <sub>3</sub>	4.49	4.59
CaO <sup>a</sup>	3.65	–

<sup>a</sup> Only for computations at  $P \geq 5$  GPa

and SiC. There are no experimental data on the Fe–Si–C ternary at high pressures; therefore, the results obtained for the Fe–Si (Brosh et al. 2009) and Fe–C (Lord et al. 2009; Rohrbach et al. 2014) binaries were used to identify phases potentially present in the Fe–Si–C ternary to 10 GPa. These phases are bcc and fcc Fe alloys, almost pure Si alloy, diamond/graphite, Fe<sub>3</sub>C, Fe<sub>7</sub>C<sub>3</sub>, FeSi, and SiC. Fe<sub>3</sub>C is the carbide coexisting with metallic Fe at low pressures, while Fe<sub>7</sub>C<sub>3</sub> is the stable liquidus phase from 10 GPa to core pressures (Shterenberg et al. 1975; Lord et al. 2009; Nakajima et al. 2009). A thermodynamic assessment of the available experimental data indicates that Fe<sub>7</sub>C<sub>3</sub> becomes stable at  $P \geq 6$  GPa, its stability expanding with pressure (Fei and Brosh in prep.). Equation of state parameters of iron carbides depends on their magnetic state (e.g., Li et al. 2002; Nakajima et al. 2011; Wood et al. 2004). The Curie temperature,  $T_c$ , of cementite is close to 210 °C at 1 bar (e.g., Tsuzuki et al. 1984), and the estimated  $T_c$  of Fe<sub>7</sub>C<sub>3</sub> lies below the temperatures of interest at high pressures; hence, for both phases we used the equation of state for the paramagnetic phase (Li et al. 2002; Wood et al. 2004; Nakajima et al. 2011). FeSi was modeled as stoichiometric phase with  $\epsilon$ -structure, consistent with the pressure range of this study (Dobson et al. 2002). Computed isothermal–isobaric compositional diagrams for the Fe–Si–C system are given in the Electronic Appendix.

The 1-bar Fe–Cr phase diagram has fcc, bcc, and  $\sigma$  Fe–Cr alloys and liquid. To reproduce phase relations at ambient pressure, we used the thermodynamic assessments of Hertzman and Sundman (1982) and Xiong et al. (2011). The formulation of the  $\sigma$ -alloy solution model of Hertzman and Sundman (1982) was employed, but end-member Gibbs free energies and excess interaction parameters were fit to two equilibrium points between the bcc and  $\sigma$ -phases at  $X_{Cr}^\sigma = 0.49$  and 0.47 at  $T = 500$  and 800 °C, respectively (Electronic Appendix). Experimental data on high-pressure phase relations in the Fe–Cr system are scarce, but two lines of evidence support the calculated high-pressure diagrams: (1) The  $\sigma$ -phase preserves its structure to 77 GPa for

**Table 3** Equation of state parameters for pure elements, alloys, intermetallic compounds, and carbides

Phase	$V^0$ (J/mol/bar)	$K_0$ (GPa)	$K'_0$	$\alpha_T = a^0 \left(1 - \frac{10}{\sqrt{T}}\right)$		References
				$a_0 (\times 10^{-5})$	$a_1 (\times 10^{-4})$	
Graphite	0.5298	39	4	4.84	-4.84	Holland and Powell (2011)
Diamond	0.342	442	4	5.4	-5.4	Dinsdale (1991), McSkimin and Andreatch (1972)
fcc Fe	0.6826	140	8	5.797	-5.797	Acet et al. (1994), Brosh et al. (2009)
fcc Si	0.896	70.7	4	0.608	-	Brosh et al. (2009), Slack and Bartram (1975)
fcc FeC	0.726	140	8	-	-	Brosh et al. (2009), Onink et al. (1993), $K_0$ and $K'_0$ as for fcc
fcc SiC	0.896	70.7	4	-	-	Parameters as for fcc Si
bcc Fe	0.705	170	6.2	2.7919	-	(Brosh et al. 2009; Müller et al. 2007)
bcc Si	0.93	71	4	0.608	-	Brosh et al. (2009)
bcc FeC	0.72	170	6.2	-	-	Brosh et al. (2009), Onink et al. (1993); $K_0$ and $K'_0$ as for bcc Fe
bcc SiC	0.93	71	4	-	-	bcc Si parameters
$\epsilon$ -FeSi	0.6745	187	5.2	4.85	-	Brosh et al. (2009)
fcc Cr	0.6826	140	8	5.797	-5.797	fcc Fe parameters
bcc Cr	1.1983	161	4.35	24,105.8	-24,105.8	Degtyareva et al. (2009), Dubrovinskaia et al. (1997), Shang et al. (2010)
$\sigma$ -Fe <sub>26</sub> Cr <sub>4</sub>	0.58035	217	5.8	2.7919	-	Degtyareva et al. (2009), coefficients for $\alpha$ as for bcc Fe
$\sigma$ -Fe <sub>10</sub> Cr <sub>20</sub>	0.58035	217	5.8	2.7919	-	Degtyareva et al. (2009), coefficients for $\alpha$ as for bcc Fe
$\beta$ -SiC	1.247	220	4	1.04105	-1.04105	Aleksandrov et al. (1989), Li and Bradt (1987)
Fe <sub>3</sub> C	2.323	174	4.8	9.7	-9.7	Li et al. (2002), Wood et al. (2004)
Fe <sub>7</sub> C <sub>3</sub>	5.282	253	3.6	8.99	-8.99	Mookherjee et al. (2011), Nakajima et al. (2011)

A full table including the calorimetric data is given in the Electronic Appendix

a bulk composition  $X_{Cr}^c = 0.49$  (Degtyareva et al. 2009); (2) the fcc phase stability field expands with pressure as predicted from ab initio calculations (Ponomareva et al. 2011). Computed  $T$ - $X_{Cr}$  diagrams for the Fe-Cr system are given in the Electronic Appendix.

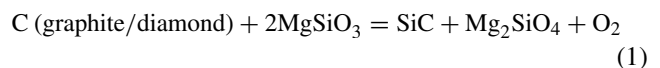
### Modifications to the thermodynamic data of silicates and oxides

For the purpose of this study, we modified the Gibbs free energy of the wüstite end-member of magnesio-wüstite given by Holland and Powell (2011) to fit the experimental determination of the iron-wüstite buffer (Campbell et al. 2009). MgO solution in magnesio-wüstite was characterized by a regular solution model with an interaction parameter  $W_{\text{fer per}} = 13$  kJ/mol (Fabrichnaya 1998). We also employ a new quaternary solution model of Cr-spinel, covering spinel ( $\text{MgAl}_2\text{O}_4$ ), hercynite ( $\text{FeAl}_2\text{O}_4$ ), and Mg-chromite ( $\text{MgCr}_2\text{O}_4$ ) components. The Gibbs free energy of Mg-chromite was estimated based on the measurements of (Klemme et al. 2009), whereas Fe-chromite was introduced as a dependent component in the solution model. Interaction coefficients were fit to experimental data of Klemme et al. (2009) and Oka et al. (1984).  $\text{Fe}^{3+}$  end-members in this solution are not considered because our concern is exclusively with conditions more reducing than the IW buffer.

## Computational results

### Phase relations of SiC at high pressure

Ulmer et al. (1998) experimentally studied the relative positions of metal-oxide buffers (Cr-Cr<sub>2</sub>O<sub>3</sub>, Mn-MnO, V-V<sub>2</sub>O<sub>3</sub>, V-VO, Ti-TiO<sub>2</sub>) and oxygen-buffering reactions involving mantle silicates to 9 GPa. These suggest that SiC forms by the reaction:



conveniently abbreviated by moissanite-olivine-opx-carbon (MOOC). Our calculations confirm that this reaction is also responsible for SiC formation in peridotites and chromitites (Figs. 1, 2). In fact, in any carbon-saturated peridotite, i.e., in the presence of graphite/diamond + olivine + opx, the  $P$ - $T$ - $f\text{O}_2$  position of this reaction will be independent of bulk composition because graphite/diamond and moissanite are pure phases and olivine and opx have  $X_{\text{Mg}} > 0.993$ .

According to Ulmer et al. (1998), the relative positions of the IW and MOOC buffers do not change much with pressure and temperature to 9 GPa and 1500 °C, the MOOC buffer remaining ~7 log units more reducing than the IW buffer. This value is similar to Mathez et al. (1995) using a simple volumetric function and calculating a  $\Delta\log f\text{O}_2[\text{IW}]$

of  $-7$  to  $-6$  at 1800 K, 0–18 GPa and confirmed by our calculations which yield a  $\Delta\log fO_2$ [IW] of  $-5.7$  to  $-12.6$  at 800–1600 °C, 0–14 GPa (Figs. 1, 2).

Furthermore, our computed silicate alloy phase relations are consistent with the experimental observations that, at 2 and 10 GPa, olivine and opx in equilibrium with SiC and Fe–Si–Ni alloy have extremely high  $X_{Mg}$  ( $X_{Mg}^{Ol} \geq 0.993$  and  $X_{Mg}^{Opx} \geq 0.995$ , Schmidt et al. 2014). In our calculations, olivine in the SiC field has negligible Fe content and Fe–Si–C alloy becomes more rich in Si with decreasing  $fO_2$  (Fig. 3).

### Phase relations in the metal-bearing mantle in terms of $P$ – $T$ – $fO_2$

Isobaric  $T$ – $fO_2$  phase diagram sections (Figs. 1, 2) for reduced metal-bearing mantle and podiform chromitite at 1, 6, and 10 GPa, illustrate how C, Fe, Cr, and ultimately Si are reduced with decreasing  $fO_2$ . These diagrams depict mineralogical changes occurring over a wide range of oxygen fugacities, from relatively oxidizing ( $fO_2 \sim$  FMQ) conditions characteristic of the uppermost mantle, through reducing ( $fO_2 \sim$  IW) conditions thought to be prevalent at  $>250$  km depth (Frost and McCammon 2008), to the ultra-reducing conditions of interest here.

The lack of data for Fe–Si–C–Cr quaternary alloy led us to make the following compromises: Since Si in the Fe–Si–C alloy remains insignificant to  $fO_2$  values where Cr-spinel reduces to metal (IW  $< -5$ ), only Fe–Cr alloys were considered at  $fO_2$  values to conditions just below chromite reduction (Fig. 1a, c, e). At more reducing conditions Fe–Cr alloys were omitted leading to a Fe–Si–C-dominated alloy composition (Fig. 1b, d, f). This omission is justified for the primitive mantle composition because of its relative low Cr content. Consequently, phase diagram sections for podiform chromitite were computed only with Fe–Cr alloys at  $fO_2$  values to the MOOC reaction (Fig. 2) where the alloy precipitating from Cr-spinel reduction should be mostly Fe–Cr rich. Nevertheless, also in the Cr-rich system SiC forms through reaction (1) which  $P$ – $T$ – $fO_2$  position is independent from the alloy composition.

Although we have formulated thermodynamic parameters for a metallic liquid in the Fe–Si–C ternary and Fe–Cr binary diagrams, a liquid phase was not included in our computations in the complex systems as data on Fe–Cr–Si–C–O metallic liquids are insufficient. As a consequence, metal melting cannot occur in our phase diagrams, although iron-dominated Fe–Si–C alloys should be molten at their upper temperature end. The lowest temperature of Fe–Si–C alloy melting can be estimated from the eutectic between fcc Fe and cementite, which lies at 1210 °C at 10 GPa (Rohrbach et al. 2014).

The uncertainties in the thermodynamic data of some alloys and intermetallic compounds result in some

uncertainty in the composition and stability of these alloys and intermetallic compounds as energetic differences between these phases are small. However, energetic differences between assemblages of different oxidation states, i.e., those containing silicate versus metal or chromite versus Fe–Cr alloy or alloy + graphite/diamond versus SiC, are large and the position of the oxygen buffer reactions is robust irrespective of the details in formulating the thermodynamics of alloys and intermetallic compounds.

### Chromite and alloy stabilities at low oxygen fugacity

The major finding from the thermodynamic calculations (Fig. 1) is that chromite and moissanite cannot coexist. Chromite reduces to metal alloy at oxygen fugacities far above those at which SiC is stabilized; this finding is independent of pressure.

#### Peridotite

Chromite reduction at a given temperature occurs at the same  $\Delta fO_2$  relative to IW: At 800 °C,  $\Delta\log fO_2$ [IW] is  $-6.6$  and  $-6.3$  at 1 and 10 GPa, respectively, and at 1600 °C  $\Delta\log fO_2$ [IW] is  $-2.0$  and  $-2.7$  at the same pressures. The resulting Fe–Cr alloy is fcc at 1 GPa and sigma phase at 10 GPa. Moissanite stability is restricted to substantially lower oxygen fugacities. At 800 °C, SiC is stabilized 12.2–12.5 log units below IW at 1 and 10 GPa, respectively; at 1600 °C  $\Delta\log fO_2$ [IW] is  $-5.7$  and  $-5.8$  at these pressures. Above the IW buffer, calculated  $X_{Cr}$  in chromite reaches 0.66, 0.79, and 1.00 at 1, 6, and 10 GPa, respectively (Fig. 3), and after the reduction and disappearance of Cr-spinel, Fe–Cr alloys become increasingly Cr rich with increasing pressure. The  $\sigma$ -phase, stable at 6 and 10 GPa, incorporates more Cr than the fcc Fe–Cr alloy stable at 1 GPa. With decreasing  $fO_2$ ,  $Fe^{2+}$  in olivine diminishes and  $X_{Mg}^{Ol}$  increases from 0.896 to 0.999 (Fig. 3). Fe–Si–C alloys become richer in Si with increasing pressure and decreasing  $fO_2$ , and  $X_{Fe}^{Fe-Si-C}$  is 0.77–0.89 at 1 GPa and decreases to 0.7 at 10 GPa.

The effect of decreasing  $fO_2$  values on Fe, Cr, Si, and C redox states for mantle compositions can be summarized as follows: At 1 GPa, cementite appears in coexistence with Cr-spinel at  $\Delta\log fO_2$ [IW]  $\approx -1$ . Chromite reduces to fcc Fe–Cr alloy at  $\Delta\log fO_2$ [IW]  $\approx -6.6$  to  $-2.8$  (800–1600 °C, Fig. 1a). At still lower  $fO_2$  values Fe–Si–C alloys (fcc and bcc) become the major Fe-bearing phases, with molar Si fractions of  $X_{Si}^{fcc} = 0.01$ – $0.11$  and  $X_{Si}^{bcc} = 0.12$ – $0.28$ . These are substituted by  $\epsilon$ -FeSi when moissanite is stabilized at  $\Delta\log fO_2$ [IW]  $\approx -9.5$  to  $-6.3$  (800–1600 °C, Fig. 1b). At 6 and 10 GPa a slightly different succession of Fe-bearing phases is established (Fig. 1c–f).  $Fe_7C_3$  becomes stable instead of  $Fe_3C$ , at  $fO_2$  values slightly above the IW

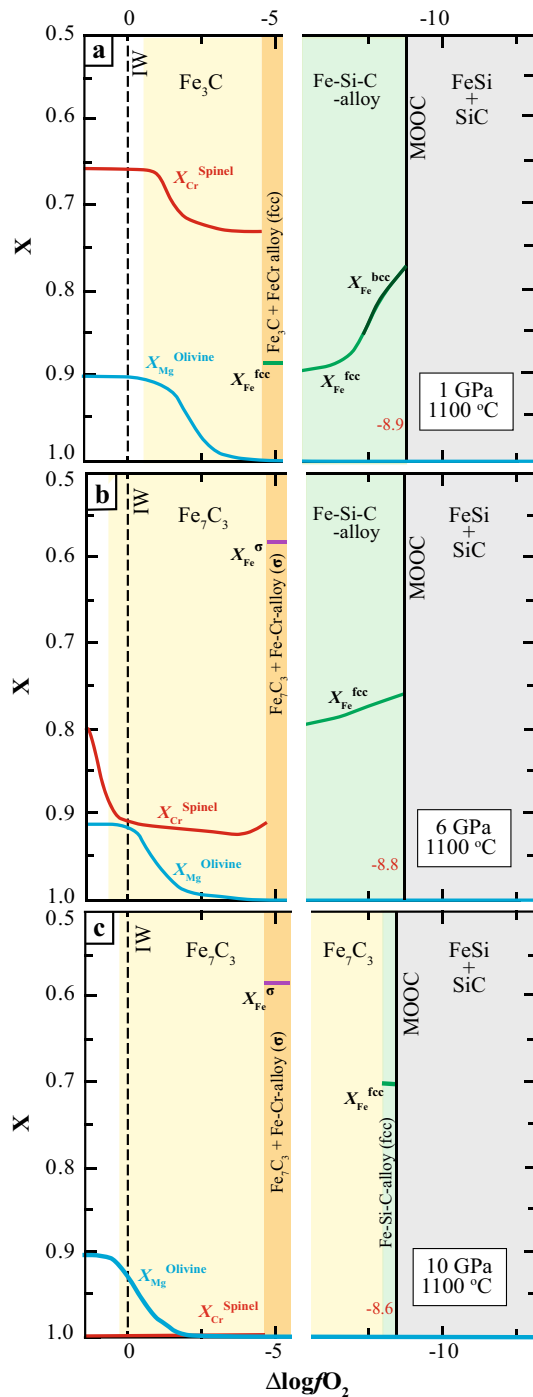


**Fig. 3** Phase compositions in the model peridotite as a function of oxygen fugacity given as  $\Delta\log fO_2$ [IW] at 1100 °C and 1, 6, and 10 GPa. Cr-spinels are characterized by an increase in  $X_{Cr}$  (= Cr/(Cr + Al)) with increasing pressure. With decreasing  $fO_2$ ,  $Fe^{2+}$  in olivine gets reduced such that at  $\Delta\log fO_2$ [IW]  $\approx -3$  to  $-5$ ,  $X_{Mg}$  (=Mg/(Mg +  $Fe^{2+}$ )) in olivine approaches 0.999. Fe–Si–C alloys become richer in Si at more reducing conditions and with increasing pressure, i.e.,  $X_{Fe}$  (=Fe/(Fe + Si + C)) decreases. In the field of SiC, stoichiometric  $\epsilon$ -FeSi compound is stable with  $X_{Si} = 0.5$ . Phase abbreviations as in Fig. 1. Note that for the peridotite composition, the calculation employs Fe–Cr alloys for about 1 log unit below the spinel breakdown and then Fe–Si–C alloys at lower oxygen fugacities (see text)

reference buffer. The reduction of chromite leads to the formation of Fe–Cr alloy in the sigma structure. Fe–Si–C alloys again occur as both fcc and bcc phases, but the field of bcc alloy significantly shrinks in comparison with 1 GPa (Fig. 1c–f).

#### Podiform chromitite

A decrease in  $fO_2$  leads to the precipitation of Fe–Cr alloy as a result of silicate and Cr-spinel reduction at  $\Delta\log fO_2$ [IW]  $\approx -1.2$  to  $-1$  at 1 to 10 GPa, with little dependency on temperature (Fig. 2). This alloy has initially less than 5 mol% Cr (Fig. 4). Cr-spinel then coexists with fcc or sigma Fe–Cr alloys over  $\sim 5$  log units. At 1 GPa, Cr contents in spinel decrease with decreasing oxygen fugacity as the Fe–Cr alloy becomes more Cr rich (Fig. 4) until an essentially Fe-free aluminous spinel with  $X_{Cr} < 0.1$  remains stable at oxygen fugacities of the MOOC buffer. The stable spinel composition in the moissanite field is then almost pure  $MgAl_2O_4$ . At pressures within the garnet stability field, chromite remains at  $X_{Cr} > 0.7$ , changes composition mainly with temperature, and decomposes to garnet and alloy at its lower oxygen fugacity stability limit. As in the phase diagram sections computed for mantle compositions,  $Fe_3C$  appears on the 1-GPa sections and  $Fe_7C_3$  becomes stable only at higher pressures. At 1 and 6 GPa, iron carbides are confined to oxygen fugacities below IW ( $\Delta\log fO_2$ [IW]  $\approx -1.2$  and  $-0.6$  at 1 and 6 GPa, respectively), whereas at 10 GPa  $Fe_7C_3$  appears in the phase assemblage at  $\Delta\log fO_2$ [IW]  $\approx 0.6$ .

## Discussion

### Thermodynamic restriction on the coexistence of chromite and SiC

Calculated phase relations (Fig. 1) show that to pressures of the mantle transition zone moissanite becomes stable at oxygen fugacities 6–13 log units more reducing than the IW buffer (Fig. 5a). In particular, along a plausible mantle geotherm, moissanite is stable at oxygen fugacities of 6.5–7 log units below IW.

The oxygen fugacity difference between the SiC-forming reaction (1) and the reduction of chromite to Fe–Cr alloy varies only slightly with pressure and temperature (Fig. 5b): For plausible mantle compositions,  $\Delta\log fO_2$  between chromite decomposition and moissanite formation is 5.6–6.8 log units at 800 °C, 1–14 GPa, and 2.9–4.9 log units at 1600 °C, 1–14 GPa the latter with a minimum difference at 2.3 GPa. This result is in agreement with the experimental determination of the relative positions of the Cr– $Cr_2O_3$  buffer and the SiC-forming reaction (Ulmer et al.

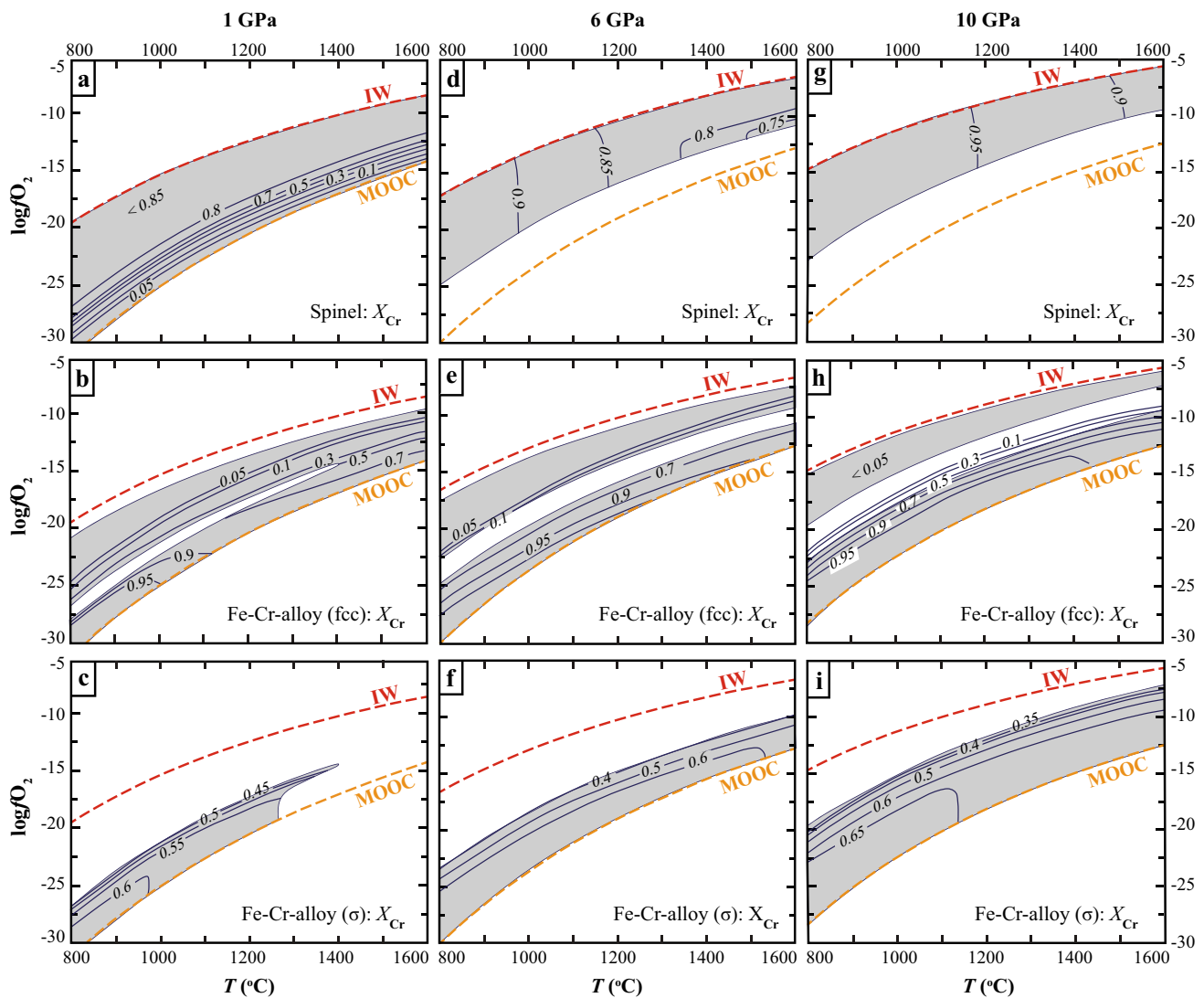


**Fig. 4** Molar spinel and alloy compositions in the chromitite model composition calculated for oxygen fugacities between the iron-wustite (IW) and the SiC-forming (MOOC) buffer reactions. *Upper row* Cr fraction in the B-site of spinel ( $X_{\text{Cr}}^{\text{spinel}} = \text{Cr}^{3+}/(\text{Al} + \text{Cr}^{3+})$ ); *middle row* Cr fraction in the fcc alloy ( $X_{\text{Cr}}^{\text{fcc}} = \text{Cr}^0/(\text{Cr}^0 + \text{Fe}^0)$ ); *bot-*

*tom row* Cr fraction in the sigma alloy ( $X_{\text{Cr}}^{\text{sigma}} = \text{Cr}^0/(\text{Cr}^0 + \text{Fe}^0)$ ). At 1 GPa, spinel does approach  $\text{MgAl}_2\text{O}_4$  composition with decreasing oxygen fugacity but does not decompose. Fe–Cr alloys increase in Cr content with decreasing  $f\text{O}_2$

1998). It suggests that (1) SiC does not stably coexist with chromite in the upper mantle, and (2) increasing pressure does not stabilize the chromite–SiC phase assemblage. Phase relations in the podiform chromitite composition differ by the fact that at 1 GPa aluminous spinel remains stable into the SiC field, but has a  $X_{\text{Cr}} < 0.05$  just above the MOOC buffer and becomes essentially pure  $\text{MgAl}_2\text{O}_4$  in the moissanite field (Fig. 4).

The results of these calculations are in good agreement with the phases observed as inclusions in or attached to natural moissanite. These phases are mostly native Si, Fe–Si alloys, or iron silicides (Di Pierro et al. 2003; Shiryayev

et al. 2011; Trumbull et al. 2009). In the Luobusa ophiolite, PGE alloys with variable amounts of Fe, Fe–Ni–Cr alloys, Cr-carbide, and iron silicide are observed (Bai et al. 2000). The PGE alloys are not unusual in chromitites (e.g., Mungall and Naldrett 2008) and compatible with oxygen fugacities in the shallow mantle.

### Hypotheses for moissanite formation

In order to explain the origin of moissanite in terrestrial rocks, a mechanism for creating an ultra-reduced environments with light carbon isotopic composition ( $\delta^{13}\text{C} = -35$

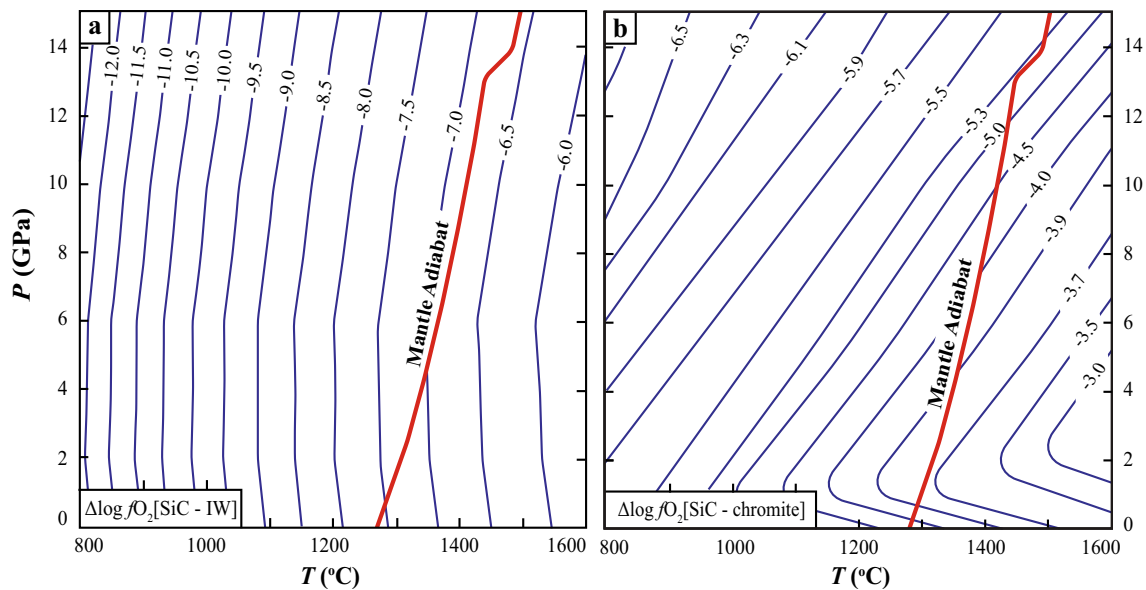


**Fig. 5** Differences in oxygen fugacity between **a** SiC stability and the iron–wustite (IW) buffer and **b** between SiC stability and chromite reduction, contoured for constant  $\Delta\log f_{\text{O}_2}$ . A 2600 J/K/kg isentrope was taken as a mantle adiabat. At upper mantle conditions, SiC becomes stable at  $f_{\text{O}_2}$  values 6.5–7.5 log units more reducing than

ambient metal-saturated mantle. Cr-spinel cannot be thermodynamically stable with moissanite because of  $\text{Cr}^{3+}$  reduction leading to the formation of Fe–Cr alloys at redox conditions 3.7–5.3 log units more oxidizing than SiC stability

to  $-18\%$ , Trumbull et al. 2009) is required. Present major hypotheses for moissanite formation include:

1. that it crystallizes at extreme pressures and temperatures, within the lower mantle or at the mantle-core boundary;
2. that it persists as a relict of the primordial ultra-reduced Earth;
3. that it originates within an anomalous global scale lower mantle reservoir characterized by low  $f_{\text{O}_2}$  and light carbon isotopic composition;
4. that it crystallizes metastably;
5. that it forms during high-pressure metamorphism of subducted carbonaceous material (Mathez et al. 1995).

The major drawbacks of these hypotheses were discussed in Mathez et al. (1995) and Trumbull et al. (2009), with an emphasis on extreme  $P$  and  $T$  conditions being essential for SiC stability. Although SiC occurs in association with diamond (Gorshkov et al. 1997; Leung 1990; Moore and Gurney 1989; Moore et al. 1986), there is no fundamental reason that it could not form at moderate  $PT$  conditions. Moreover, the stability of diamond does not necessarily require  $P > 5$  GPa if temperatures are relatively low (the computed graphite–diamond phase boundary is at 760–1027 °C at 3.5–5 GPa).

The first step in understanding the origin of SiC within chromitites would be to analyze the textural relations between chromite and moissanite grains; however, SiC is reported only

from heavy mineral concentrates and SiC and chromite have not been observed in direct contact in intact rocks (Robinson et al. 2004; Trumbull et al. 2009). Our thermodynamic analysis is clear in that SiC cannot stably coexist with chromite (Figs. 1, 2), and moissanite only becomes stable at redox conditions 3.7–5.3 log units lower than the chromite–Fe–Cr alloy equilibrium (Fig. 5). Predictions of the redox state in the lower mantle are based on the fact that Mg-perovskite incorporates significant amounts of  $\text{Fe}^{3+}$ , leading to  $\sim 1$  wt% metallic Fe in the lower mantle. Assuming a constant amount of oxygen for the upper and lower mantle, this constrains the lower mantle  $f_{\text{O}_2}$  to  $\Delta\log f_{\text{O}_2}[\text{IW}] = 0$  to  $-1.5$  (Frost and McCammon 2008). Therefore, also lower mantle redox conditions are far too oxidizing to stabilize SiC. Moreover, if moissanite-permitting low  $f_{\text{O}_2}$  values were widespread in the deep Earth, such domains would be characterized by  $X_{\text{Mg}}$  values of 0.993–0.999 in coexisting silicates (Schmidt et al. 2014). Such  $X_{\text{Mg}}$  values have never been reported, also not as inclusions in diamonds.

### A new model for moissanite formation in peridotites

Chromite and moissanite cannot be in equilibrium, but SiC is reported from heavy mineral concentrates from ophiolitic chromitites. There are, hence, two possibilities: (1) SiC formed before chromite, or (2) chromite formed before SiC, and (2a) the entire rock volume was subject to

oxygen fugacities of the moissanite-buffer or (2b) moissanite formed on a grain scale microenvironment at temperatures where larger-scale equilibration did not occur.

(1) Podiform chromitites form through precipitation of chromite from H<sub>2</sub>O-bearing silicate melts at temperatures above the mantle solidus, at least at 1000–1200 °C (Ballhaus 1998). Cr solubilities in silicate melts are low (~0.2 wt%, Cameron 1985; Khedim et al. 2010; Poustovetov and Roeder 2001), and only a small fraction of the dissolved Cr could be precipitated due to changes in pressure, temperature, or melt composition (including redox state). Consequently, the precipitation of up to 80 % chromite in a given rock volume requires percolation of melt volumes at least several hundred times those of the chromite. It is thus difficult to conceive how, in such an intense magmatic environment at >1000 °C, SiC should survive metastably; therefore, we dismiss this possibility.

(2a) Subjecting podiform chromitites to oxygen fugacities of the moissanite-buffer would require reducing all Fe<sup>2+</sup> to Fe<sup>0</sup> and all Cr<sup>3+</sup> to Cr<sup>0</sup>. A 50:50 chromite–dunite mixture contains ~38.8 wt% O, and reduction of all Fe and Cr would, by simple mass balance, liberate 11.6 wt% O from the rock (chromite composition from Yamamoto et al. (2009), dunite from Zhou et al. (1996)). The Cr-spinel component as well as the Fe components of the silicates would recrystallize as metals and silicides, and 11.6 wt% O would have to be removed from the rock. After moissanite formation, the oxygen would have to be added back (presumably through melts or fluids) and the metal(s) and silicides would need to crystallize back to the typical texture of podiform chromitites, without any trace of the massive metasomatism required to refurbish in oxygen, and without re-equilibrating the moissanite. This scenario appears fairly implausible as it requires massive oxygen fluxes.

(2b) The simplest solution to the above dilemma is that moissanite forms after chromite, in a microenvironment at temperatures where diffusion does not reach beyond the grain scale and where the temperatures of reaction are insufficient to have the oxygen fugacity of the microenvironment influencing the chromite and majority of silicates. In the following we discuss a mechanism where the migration of fluids, probably along grain boundaries or extremely restricted zones, may result in moissanite. Support for the involvement of fluids comes from the observation that moissanite occurs within serpentinites and brucite-bearing rocks: SiC was documented in situ as a minor phase in serpentinites (Xu et al. 2008) or even as rock-forming mineral in a brucite-rich rock (Di Pierro et al. 2003).

### Fluid evolution and the formation of ultra-reduced microenvironments

Crystallization of phases at reducing and ultra-reducing conditions may be mediated by a fluid strongly depleted in

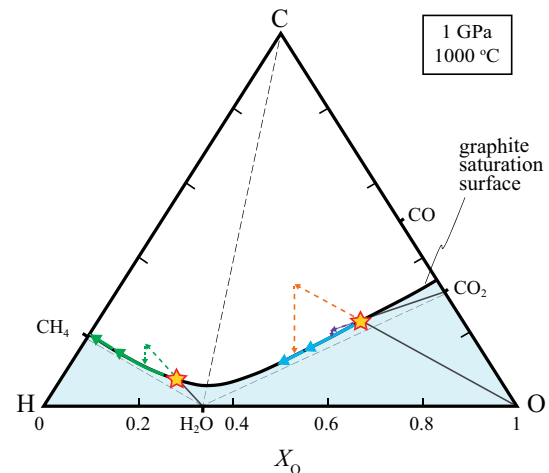


**Fig. 6** Isobaric–isothermal ( $P = 1$  GPa,  $T = 1000$  °C) compositional diagram for graphite-saturated C–O–H fluids, schematically illustrating mechanisms removing oxygen from the fluid. The compositional variable  $X_O$  represents the atomic fraction  $O/(O + H)$  in the fluid. The graphite saturation surface was calculated after Connolly and Cesare (1993) possible fluid compositions are in the blue field. Consider two graphite-saturated initial fluid compositions (stars) either on the left- or right-hand side of the C–H<sub>2</sub>O join (dashed black line). The fluid composition changes from relatively reduced to ultra-reduced (green arrows), when hydrous minerals (talc, brucite, serpentine) formed from olivine and orthopyroxene sequester H<sub>2</sub>O from the fluid. More oxidized fluid compositions (star to the right), carbonate formation (blue arrows), or Fe<sup>2+</sup> oxidation, such as magnetite formation (orange arrows), also leads to fluid depletion in oxygen and may move initial fluid compositions to the more reducing side of the C–H<sub>2</sub>O tie line. The arrows reaching into the C-saturated field illustrate the O-removal as a two-step process (mineral formation either removing H<sub>2</sub>O, CO<sub>2</sub>, or O<sub>2</sub> from the fluid) followed by graphite precipitation which moves the fluid back to the graphite saturation surface. In nature these steps are concomitant or almost infinitesimal small

oxygen (Fig. 6). We propose that the formation of such fluids is a gradual process involving two steps. In a first step a fluid more reducing than the H<sub>2</sub>O–C tie line is required, and in a second step this fluid evolves to ultra-reducing compositions by removal of H<sub>2</sub>O through formation of hydrous minerals.

### The origin of moderately reducing fluids

The easiest way to obtain a moderately reduced fluid is the metamorphic devolatilization of sediments rich in organic material. Kerogen-rich material would supply graphite-saturated fluids with an  $X_O < 0.33$  that plot to the left of the H<sub>2</sub>O–C tie line in Fig. 6. Alternatively, an oxygen depletion of the fluid can be realized by retrograde carbonate or magnetite formation. These minerals would remove oxygen from the fluid and drive its composition away from CO<sub>2</sub> or O<sub>2</sub> along the graphite/diamond-saturation surface toward lower  $X_O$ , as indicated by arrows on Fig. 6.

To illustrate this mechanism of fluid reduction, we computed  $T$ – $X_O$  diagrams for MgO–C–H–O at 0.2 and 1 GPa

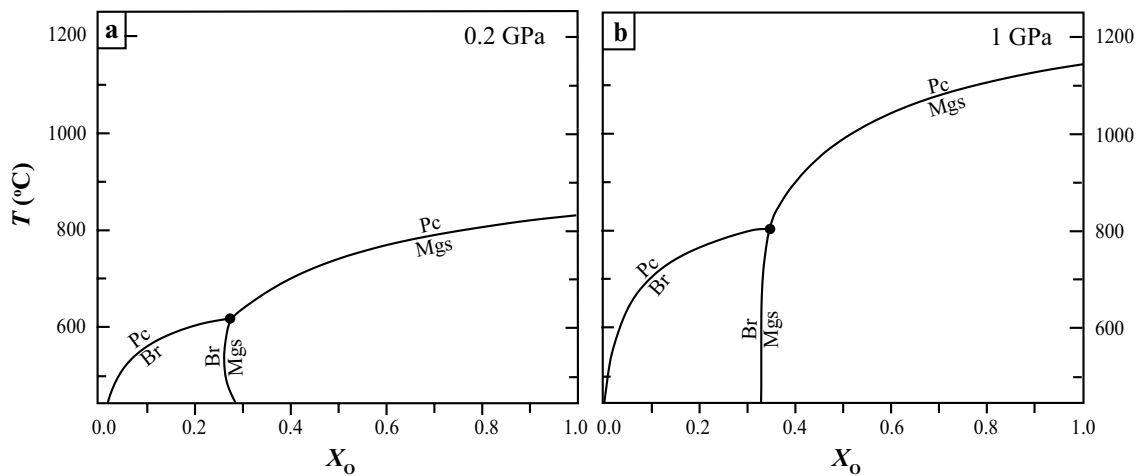
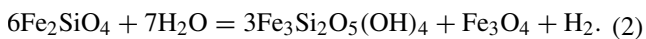


**Fig. 7**  $T$ - $X_{\text{O}}$  diagrams calculated for the carbon-saturated model MgO-C-O-H system at  $P = 0.2$  and 1 GPa. With decreasing temperature, magnesite + periclase saturation buffers the fluid composi-

tion toward  $X_{\text{O}} < 1/3$  only at 0.2 (a), where magnesite is succeeded by brucite, stable down to  $X_{\text{O}} = 0.02$  and 0.001 at 0.2 and 1 GPa (a, b), respectively. Br—brucite; Mgs—magnesite; Pc—periclase

(Fig. 7). Magnesite is stable down to  $X_{\text{O}} = 0.29$  at relatively low pressures ( $P = 0.2$  GPa, Fig. 7a), and its formation will move fluid compositions to this value, i.e., to the reduced side of the C-H<sub>2</sub>O tie line (Fig. 6). In this simple model system, magnesite is only stable at  $X_{\text{O}}$  values  $> 0.33$  at higher pressures (1 GPa, Fig. 7b). In this case, initial fluid compositions would be required to lie already on the reduced side of the C-H<sub>2</sub>O tie line in order to develop to ultra-reduced compositions.

A third alternative that leads to oxygen-depleted fluids is magnetite formation. A suitable reaction occurs commonly during serpentinization, where  $X_{\text{Mg}}$  serpentine is generally greater than  $X_{\text{Mg}}$  olivine causing magnetite to precipitate (e.g., Moody 1976; Ramdohr 1967) according to



This reaction is known to lead to H<sub>2</sub>-rich fluids (Sleep et al. 2004), Fe<sup>2+</sup> oxidation consuming O<sub>2</sub> from the fluid. This type of mechanisms may suffice to drive fluid compositions to an  $X_{\text{O}} < 0.33$ .

Fundamentally, there is no restriction on pressures at which moderately reducing fluids could form through any of the above three processes. Thus, initial C-O-H fluids could originate in subduction zones but equally during orogenesis. Ophiolites hosting podiform chromitite bodies bear evidence for modification within a suprasubduction environment (Malaspina et al. 2010).

#### *The fractionation of moderately reducing to ultra-reducing fluids*

Any fluid with  $X_{\text{O}} < 0.33$  will evolve to more reduced compositions when removing H<sub>2</sub>O from the fluid through

forming hydrous phases (Connolly 1995). In the mantle, such hydrous phases could form by reaction of olivine and/or orthopyroxene to, e.g., talc, serpentine, or brucite or at higher pressures to, e.g., phase A or the 10 Å phase (Fumagalli and Poli 2005). Figure 7 illustrates this principle in the simple MgO-C-H-O model system, where brucite formation leads to fluids which evolve toward very low  $X_{\text{O}}$  of 0.02–0.001 at 430 °C and 0.2–1 GPa, respectively.

Alternatively, the fluid might simply not react with its surroundings at all but crystallize hydrous phases from dissolved oxide components (e.g., SiO<sub>2</sub>, MgO). In such a scenario, the fluid evolves by itself, simply precipitating hydrous minerals (and other dissolved matter) upon rise and cooling.

Among the suitable hydrous minerals for oxygen sequestration from the fluid, brucite has the highest temperature stability of 850–970 °C at 1–2 GPa (Johnson and Walker 1993). On the  $T$ - $X_{\text{O}}$  phase diagram section computed at 1 GPa for carbon-saturated MgO-C-H-O systems (Fig. 7), the highest temperature of brucite stability is confined to 717 °C and  $X_{\text{O}} \sim 0.3$ . Therefore, 700 °C is about the upper temperature limit of extreme fluid fractionation, and also serpentine in mantle compositions is limited to  $\sim 700$  °C.

A decrease in the fluid's  $X_{\text{O}}$  in the course of depletion in oxygen will inevitably change its speciation (Fig. 8). The maximum concentration of H<sub>2</sub>O ( $y_{\text{H}_2\text{O}}$ ) occurs at the water maximum at  $X_{\text{O}} = 1/3$ , and further decrease in  $X_{\text{O}}$  results in more CH<sub>4</sub>-rich compositions. At  $f\text{O}_2$  values corresponding to moissanite stability, fluids are expected to be mostly CH<sub>4</sub> with little H<sub>2</sub>O and H<sub>2</sub>. On the 1 GPa  $\log(y_i)$ - $X_{\text{O}}$  diagram, calculated changes in fluid speciation are smoother at 1000 °C than at 423 °C (Fig. 8). Moreover, there are two solvi on the CH<sub>4</sub>-H<sub>2</sub>O join, and the one toward the more

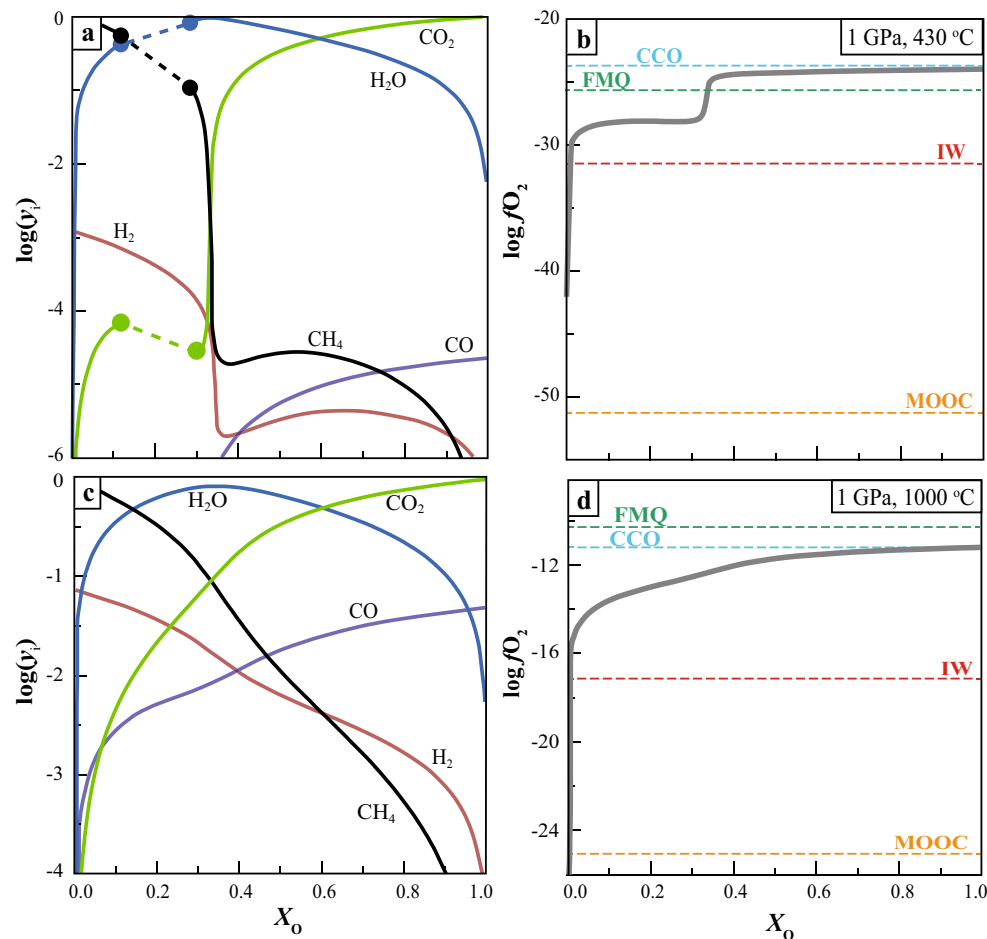


**Fig. 8** Calculated speciation (**a, c**) and  $\log fO_2$  (**b, d**) of graphite-saturated C–O–H fluids at 1 GPa and 427, **a, b**, and 1000 °C. **c, d**. Horizontal lines on the  $\log fO_2$ – $X_O$  diagram represent the location of the reference CCO, FMQ, IW, and MOOC buffers. Depending on  $\log fO_2$

fluid speciation changes from mostly  $CO_2$  rich at oxidizing conditions toward  $CH_4$  rich at reducing conditions. The immiscibility in the  $CH_4$ – $H_2O$ -dominated compositions at  $P = 1$  GPa and  $T = 427$  °C is indicated by the dashed lines (**a**) on the discontinuous  $\log(y_i)$  curves

reducing side closes only at  $\sim 467$  °C (Electronic Appendix). The formation of two conjugate fluids, one more  $H_2O$  rich and one more  $CH_4$  rich, does not lead to different  $fO_2$  values as their  $\mu_O$  values must be equal. Nevertheless, once physically separated, the more reduced fluid may develop more readily to ultra-reducing compositions.

Several observations support a scenario where oxygen fractionation out of fluid locally affects redox conditions in the mantle, and particularly, that this mechanism leads to ultra-reduced microenvironments: A substantial role of fluids for SiC precipitation can be deduced from the in situ findings of moissanite in rocks largely comprised of brucite or serpentine (Di Pierro et al. 2003; Xu et al. 2008). Secondly, an involvement of fluids in the processes related to podiform chromitite formation is indicated by paragenetic amphibole and phlogopite inclusions in chromites (Auge 1987; Johan et al. 1983; Matveev and Ballhaus 2002; Peng et al. 1995).

### Effect of fluid fractionation on carbon isotope composition

The moissanites analyzed for C-isotopes are characterized by light carbon compositions with  $\delta^{13}C = -35$  to  $-18$  ‰ for occurrences in podiform chromitites (Trumbull et al. 2009),  $-27$  to  $-24$  ‰ for moissanites from kimberlites (Mathez et al. 1995), and  $-26.7 \pm 3.4$  ‰ for the SiC-bearing pebble found in Turkey (Trumbull et al. 2009).

Starting with a fluid on the graphite saturation surface with  $X_O = 0.3$ , about 1 mol% of graphite precipitates when the fluid evolves to  $X_O < 0.01$ , its composition changing from a molar  $CH_4:H_2O:CO_2:H_2$  of 8.3:90.6:0.8:0.3 to 98:0.4:0:1.6 (1 GPa, 700 °C). With the relevant isotope fractionations being  $\Delta^{13}C_{\text{graphite-}CH_4} \approx 2.3$  ‰;  $\Delta^{13}C_{CO_2\text{-graphite}} \approx 5.4$  ‰; and  $\Delta^{13}C_{CO_2\text{-calcite}} \approx 2.3$  ‰ (Bottinga 1969), Rayleigh fractionation would lower  $\delta^{13}C_{\text{fluid}}$  from 0 to  $-0.02$  ‰, the precipitating graphite progressing from

1.46 to 2.28 ‰ in composition. Consequently, an ultra-reducing fluid with  $\delta^{13}\text{C} \sim -20$  ‰ requires an initial fluid with a similar  $\delta^{13}\text{C}$  value. Isotope fractionation factors between moissanite and  $\text{CH}_4$  are unknown but are expected to be in the order of a few per mille (in analogy to graphite and diamond). Hence, to obtain SiC with  $\delta^{13}\text{C}_{\text{SiC}} = -35$  to  $-18$  ‰, starting fluids should be similarly light, strongly supporting a C-origin from organic sedimentary material, which has typically  $\delta^{13}\text{C}_{\text{Org}} = -30$  to  $-10$  ‰ (Faure and Mensing 2005).

The above calculation considers the case where fluids evolve through removal of  $\text{H}_2\text{O}$  through mineral hydration. It is useful to evaluate the two other mechanisms that lead oxidized fluids to become moderately reduced. If oxygen is removed from the fluid through oxidation of  $\text{Fe}^{2+}$ , e.g., by forming magnetite during serpentinization, the fluid coprecipitates graphite (Fig. 6, see also Connolly 1995). Such fluids have  $\text{CO}_2 > \text{CH}_4$ , and the graphite is isotopically lighter than the fluid, which then evolves to isotopically heavier compositions. Similar, when precipitating carbonate from a  $\text{CO}_2$ -rich fluid, the fluid becomes isotopically heavier. Consequently, fluid reduction through carbonate or magnetite precipitation results in isotopically heavier fluids, contrasting the fairly light SiC carbon isotope compositions.

We note that the range of  $\delta^{13}\text{C}$  in graphite from meteorites is  $-50$  to  $+340$  (Faure and Mensing 2005), and hence, primordial carbon could in principal also provide the light  $\delta^{13}\text{C}$  values of terrestrial moissanite. However, primordial SiC could not survive in the convective mantle, and diffusive equilibration at adiabatic temperatures would destroy any ultra-reduced phase within millions of years.

### Formation conditions of SiC in the Luobusa ophiolite

A deep mantle stage of 100 km or possibly as much as 380 km depth was proposed for the moissanite-bearing podiform chromitites from the Luobusa ophiolite (Robinson et al. 2004; Yamamoto et al. 2009), although it is generally believed that podiform chromitites form as a result of magmatic processes in the uppermost mantle (e.g., Ballhaus 1998). The postulated high pressures are based on coesite–kyanite intergrowth around Fe–Ti alloys (Yang et al. 2007; for a summary see Liou et al. 2014) and on nanoscale coesite and diopside exsolution lamellae in chromite grains. To explain an increased solubility of Ca and Si in the chromite, Yamamoto et al. (2009) speculated that Cr-spinel crystallized originally as  $\text{CaFe}_2\text{O}_4$  (CF) phase, which requires 12.8 GPa (Chen et al. 2003; Yamamoto et al. 2009). Nevertheless, a quantitative assessment of the reintegrated original concentration of Ca and Si in the chromite is not provided, and as an alternative explanation, a decrease of Ca and Si solubilities in chromite with

decreasing temperature or changing oxygen fugacity (Buddington and Lindsley 1964) would be sufficient to explain the tiny volume of these exsolutions. Regardless of this consideration, SiC is not stable with chromite; therefore, chromite reduction to a Fe–Cr alloy would be inevitable if moissanite were to form under equilibrium conditions.

A further argument against pervasive high-pressure metamorphism of the podiform chromitites in the Luobusa and Dongqiao, Semail, and Ray-Iz ophiolites is the almost complete absence of garnet in these rocks. It is in fact inconceivable, how these rocks could have re-equilibrated in the garnet stability field (or even in the CF stability field), then re-entered and recrystallized in the spinel stability field and still preserve the original textures characteristic for podiform chromitites. The occasional microgarnets (Robinson et al. 2004, Liou et al. 2014) are in fact very much in line with an extremely limited recrystallization of these rocks at eclogite facies conditions. Whatever, re-crystallizing of the entire rock from garnet to chromite facies would leave no chance for preservation of SiC if not armored by an inert mineral.

At face value, the requirements to satisfy the different minerals in the Luobusa chromitites are met at 3.5 GPa,  $\sim 700$  °C: This pressure–temperature condition is in the coesite field (exsolutions in chromite, Yamamoto et al. 2009), in the diamond stability field (diamonds from heavy mineral concentrates, e.g., Bai et al. 2000), at the limit of serpentine stability, and at temperatures which would allow for the preservation of SiC grains. Diffusive equilibration of SiC with the FeMg silicates would destroy mm-sized SiC grains within less than 1 Myrs at  $\geq 800$  °C (Schmidt et al. 2014).

A condition of 3.5 GPa,  $\sim 700$  °C is easily satisfied if a suprasubduction ophiolite, a setting consistent with podiform chromite-forming mechanisms, is entrained to moderate depths of 110 km where 700 °C is realistic in the vicinity of the slab. The slab could then provide the reduced fluids that will ultimately lead to SiC precipitation on grain boundaries. We speculate that the few diamonds found in several tons of processed chromitite formed from the reduced C-bearing fluids passing through the rock. In fact the evolution of the fluids from moderately to ultra-reduced causes continuous precipitation of carbon. As both moissanite and diamond have the same light  $\delta^{13}\text{C}$  signature far from average mantle values, a single source of carbon appears well likely.

A reducing environment is also consistent with the large range of carbides, silicides, base metal alloys, and native Si described by Bai et al. (2000) and Liou et al. (2014). The occurrence of small amounts of Cr-rich alloys and a Cr-carbide provides further evidence that chromite is not stable at the ultra-reduced conditions permitting SiC. The panoply of ultra-reduced phases in mineral separates of

the podiform chromitites that have moissanite (Trumbull et al. 2009) demonstrates that the bulk of these rocks, i.e., the silicates (with  $X_{Mg}$ 's near 0.9) and the chromite, is not in equilibrium with these phases. This feature is well explained with ultra-reducing conditions being limited to grain boundaries at temperatures where diffusional equilibration is extremely limited.

## Conclusions

Experiments (Schmidt et al. 2014), end-member thermodynamic calculations (Ulmer et al. 1998), and complex thermodynamic modeling of natural bulk compositions (this study) all demonstrate that oxygen fugacities allowing for SiC require Fe and Cr to be reduced at least to their native state. Minerals in equilibrium with SiC could only contain traces of  $Fe^{2+}$  or  $Cr^{3+}$ . Our calculations show that moissanite and chromite do not stably coexist and that increasing pressure does not increase the stability of this mineral pair (Fig. 5). For plausible mantle conditions, chromite is reduced to Fe–Cr alloy at  $fO_2$  values 3.7–5.1 log units above those where SiC becomes stable in presence of mantle silicate (i.e., the MOOC buffer), and this  $\Delta \log fO_2$  increases slightly with decreasing temperature and increasing pressure.

If large regions characterized by ultra-reducing conditions (and by light carbon isotope composition) were present in the Earth's mantle, these would have olivines and pyroxenes with  $X_{Mg} > 0.99$ , as all iron in the stability field of SiC will be contained in Fe-based alloys and/or iron silicides. The general absence of such high  $X_{Mg}$  silicates indicates that moissanite originates from ultra-reduced microenvironments.

Ultra-reducing fluids may form from graphite-/diamond-saturated moderately reducing fluids by removal of  $H_2O$ , to be structurally bound into hydrous phases (serpentine, brucite, phase A). Hydrous phases could be formed during hydration of peridotites, but could also simply precipitate from the solute in the fluid. Carbon isotope compositions indicate that such moderately reducing fluids would derive from organic-rich sediments and findings of SiC within rocks consisting mostly of serpentine and brucite support this model and indicate <700–800 °C. Such temperatures would allow for SiC formation in restricted ultra-reduced zones where fluids infiltrate but where diffusive equilibration of the host rock minerals with the fluid does not take place. This mechanism does not directly constrain pressure, but the limitation in temperature indicates that SiC could only form in cold lithospheric mantle keels, in the vicinity of subducting slabs, or during orogenesis.

Models where SiC-bearing rocks are formed at transition zone depths and/or in plume environments have to be

rejected. The problem with large depths is the high temperature and the bulk rock equilibration following from such temperatures. The concept of oxygen fugacity may unfortunately be mistaken such that oxygen fugacity is interpreted as a free variable. This is not the case. The bulk oxygen content of a rock changes little between oxygen buffers but dramatically across oxygen buffers. Crossing from oxygen fugacities at the iron–wustite buffer to the moissanite–olivine–opx–carbon MOOC buffer would require any mantle rock to shed 2 wt% oxygen (all Fe reduced to alloys, carbides, or silicides) and an average podiform chromitite to shed 12 wt% oxygen. A podiform chromitite can hence not equilibrate in the SiC stability field without losing this amount of oxygen; even worse, it would have to regain the same amount of oxygen during its way back to chromite stability.

All of the above is resolved if the SiC is formed from a fluid percolating along grain boundaries or along narrow zones in disequilibrium with the bulk rock, necessarily involving moderate temperatures.

Moissanite could be protected from diffusive equilibration with the surroundings by diamond, the only known adequate armor in mantle compositions. If diamond grows and encapsulates moissanite, possibly from the same fluid, then these moissanite inclusions would remain stable over time and at higher temperatures. Chromite- or Fe-bearing silicates are unsuitable hosts as these are in redox disequilibrium with moissanite.

SiC is also described from kimberlites and other volcanic rocks (Shiryaev et al. 2011; Kaminsky et al. 2016). Such SiC could simply be picked up upon magma ascent; alternatively, fluid-mediated SiC formation and eruption could be linked. Nevertheless, the magma (with FeO contents typical for basaltic rocks) could not be in equilibrium with SiC, but fast exhumation and cooling would allow for higher temperatures of SiC formation. Diamond and SiC in such rocks may also precipitate at low pressures from a gas phase (Kaminsky et al. 2016) that must remain chemically isolated from the bulk rock.

**Acknowledgments** This study was financed through Grants 200020-140541/1 and 200020-153112/1 by the Swiss National Science Foundation. We thank L. Dobrzhinskaya, M.F. Zhou, and an anonymous reviewer for critical remarks that helped very much sharpening the manuscript.

## References

- Acet M, Zähres H, Wassermann EF (1994) High-temperature moment-volume instability and anti-Invar of g-Fe. *Phys Rev B Condens Matter Mater Phys* 49:6012–6017
- Aleksandrov IV, Goncharov AF, Stishov SM, Yakovenko EV (1989) Equation of state and Raman scattering in cubic BN and SiC at high pressures. *J Mater Sci* 50:127–131

- Auge T (1987) Chromite deposits in the northern Oman ophiolite: mineralogical constraints. *Miner Deposita* 22:1–10
- Bai WJ, Robinson PT, Fang QS, Yang JS, Yan BG, Zhang ZM, Hu XF, Zhou MF, Malpas J (2000) The PGE and base-metal alloys in the podiform chromitites of the Luobusa ophiolite, southern Tibet. *Can Mineral* 38:585–598
- Ballhaus C (1998) Origin of podiform chromite deposits by magma mingling. *Earth Planet Sci Lett* 156:185–193
- Ballhaus C, Berry RF, Green DH (1991) High-pressure experimental calibration of the olivine–orthopyroxene–spinel oxygen geobarometer: implications for the oxidation state of the upper mantle. *Contrib Miner Petrol* 107:27–40
- Bottinga Y (1969) Calculated fractionation factors for carbon and hydrogen isotope exchange in system calcite–carbon dioxide–methane–hydrogen–water vapor. *Geochimica Et Cosmochimica Acta* 33:49–64
- Brosh E, Makov G, Shneck RZ (2009) Thermodynamic analysis of high-pressure phase equilibria in Fe–Si alloys, implications for the inner-core. *Phys Earth Planet Inter* 172:289–298
- Buddington AF, Lindsley DH (1964) Iron–titanium oxide minerals and synthetic equivalents. *J Petrol* 5:310–357
- Cameron WE (1985) Petrology and origin of primitive lavas from the Troodos ophiolite, Cyprus. *Contrib Miner Petrol* 89:239–255
- Campbell AJ, Danielson L, Richter K, Seagle CT, Wang Y, Praka-penka VB (2009) High pressure effects on the iron–iron oxide and nickel–nickel oxide oxygen fugacity buffers. *Earth Planet Sci Lett* 286:556–564
- Chen M, Shu J, Mao HK, Xie X, Hemley RJ (2003) Natural occurrence and synthesis of two new postspinel polymorphs of chromite. *Proc Natl Acad Sci* 100:14651–14654
- Connolly JAD (1995) Phase diagram methods for graphitic rocks and application to the system C–O–H–FeO–TiO<sub>2</sub>–SiO<sub>2</sub>. *Contrib Miner Petrol* 119:94–116
- Connolly JAD (2009) The geodynamic equation of state: what and how. *Geochem Geophys Geosyst*. doi:10.1029/2009GC002540
- Connolly JAD, Cesare B (1993) C–O–H–S fluid composition and oxygen fugacity in graphitic metapelites. *J Metamorph Geol* 11:379–388
- Dasgupta R, Hirschmann MM (2010) The deep carbon cycle and melting in Earth's interior. *Earth Planet Sci Lett* 298:1–13
- Degtyareva VF, Dubrovinsky L, Kurnosov A (2009) Structural stability of the sigma phase FeCr under pressure up to 77 GPa. *J Phys Condens Matter* 21:1–4
- Deines P (2002) The carbon isotope geochemistry of mantle xenoliths. *Earth Sci Rev* 58:247–278
- Di Pierro S, Gnos E, Grobety BH, Armbruster T, Bernasconi SM, Ulmer P (2003) Rock-forming moissanite (natural alpha-silicon carbide). *Am Mineral* 88:1817–1821
- Dinsdale AT (1991) SGTE data for pure elements. *CALPHAD* 15:317–425
- Djurovic D, Hallstedt B, von Appen J, Dronskowski R (2011) Thermodynamic assessment of the Fe–Mn–C system. *CALPHAD* 35:479–491
- Dobson D, Vočadlo L, Wood IG (2002) A new high-pressure phase of FeSi. *Am Mineral* 87:784
- Dubrovinskaia NA, Dubrovinsky LS, Saxena SK, Sundman B (1997) Thermal expansion of chromium (Cr) to melting temperature. *CALPHAD* 21:497–508
- Fabrichnaya O (1998) The assessment of thermodynamic parameters for solid phases in the Fe–Mg–O and Fe–Mg–Si–O systems. *CALPHAD* 22:85–125
- Faure G, Mensing TM (2005) *Isotopes, principals and applications*, 3rd edn. Wiley, Hoboken
- Frost DJ, McCammon CA (2008) The redox state of Earth's mantle. *Annu Rev Earth Planet Sci* 36:389–420
- Fumagalli P, Poli S (2005) Experimentally determined phase relations in hydrous peridotites to 6.5 GPa and their consequences on the dynamics of subduction zones. *J Petrol* 46:555–578
- Gorshkov AI, Bao YN, Bershov LV, Ryabchikov ID, Sivtsov AV, Lapina MI (1997) Inclusions of native metals and other minerals in diamond from Kimberlite pipe 50, Liaoning, China. *Geokhimiya* 8:794–804
- Gustafson P (1985) A thermodynamic evaluation of the Fe–C system. *Scand J Metall* 14:259–267
- Hertzman S, Sundman B (1982) A thermodynamic analysis of the Fe–Cr system. *CALPHAD* 6:67–80
- Holland TJB, Powell R (2011) An improved and extended internally consistent thermodynamic dataset for phases of petrological interest, involving a new equation of state for solids. *J Metamorph Geol* 29:333–383
- Irvine TN (1965) Chromian spinel as a petrogenetic indicator; Part 1, theory. *Can J Earth Sci* 2:648–672
- Johan Z, Dunlop H, Lebel L, Robert JL, Völtinger M (1983) Origin of chromite deposits in ophiolitic complexes: evidence for a volatile and Na-rich reducing fluid phase. *Fortschr Mineral* 61:105–107
- Johnson MC, Walker D (1993) Brucite Mg(OH)<sub>2</sub> dehydration and the molar volume of H<sub>2</sub>O to 15 GPa. *Am Mineral* 78:271–284
- Kaminsky FV, Wirth R, Anikin LP, Morales L, Schreiber A (2016) Carbonado-like diamond from the Avacha active volcano in Kamchatka, Russia. *Lithos*. doi:10.1016/j.lithos.2016.02.021
- Khedim H, Podor R, Panteix PJ, Rapin C, Vilasi M (2010) Solubility of chromium oxide in binary soda–silicate melts. *J Non Cryst Solids* 356:2734–2741
- Klein-BenDavid O, Logvinova AM, Schrauder M, Spetius ZV, Weiss Y, Hauri EH, Kaminsky FV, Sobolev NV, Navon O (2009) High-Mg carbonatitic microinclusions in some Yakutian diamonds—a new type of diamond-forming fluid. *Lithos* 112:648–659
- Klemme S, Ivanic TJ, Connolly JAD, Harte B (2009) Thermodynamic modelling of Cr-bearing garnets with implications for diamond inclusions and peridotite xenoliths. *Lithos* 112:986–991
- Kopylova M, Navon O, Dubrovinsky L, Khachatryan G (2010) Carbonatitic mineralogy of natural diamond-forming fluids. *Earth Planet Sci Lett* 291:126–137
- Lacaze J, Sundman B (1991) An assessment of the Fe–Si–C system. *Metall Trans A* 22A:2211–2223
- Leung IS (1990) Silicon carbide cluster entrapped in a diamond from Fuxian, China. *Am Mineral* 75:1110–1119
- Li Z, Bradt RC (1987) Thermal expansion of the hexagonal (4H) polype of SiC. *J Am Ceram Soc* 70:445–448
- Li J, Mao HK, Fei Y, Gregoryanz E, Eremets M, Zha CS (2002) Compression of Fe<sub>3</sub>C to 30 GPa at room temperature. *Phys Chem Miner* 29:166–169
- Liou JG, Tsujimori T, Yang J, Zhang RY, Ernst WG (2014) Recycling of crustal materials through study of ultrahigh-pressure minerals in collisional orogens, ophiolites, and mantle xenoliths: a review. *J Asian Earth Sci* 96:386–420
- Lord OT, Walter MJ, Dasgupta R, Walker D, Clark SM (2009) Melting in Fe–C system to 70 GPa. *Earth Planet Sci Lett* 284:157–167
- Malaspina N, Scambelluri M, Poli S, Van Roermund HLM, Langenhorst F (2010) The oxidation state of mantle wedge majoritic garnet websterites metasomatised by C-bearing subduction fluids. *Earth Planet Sci Lett* 298:417–426
- Mathez EA, Fogel RA, Hutcheon ID, Marshintsev VK (1995) Carbon isotopic composition and origin of SiC from kimberlites of Yakutia, Russia. *Geochim Cosmochim Acta* 59:781–791
- Matveev S, Ballhaus C (2002) Role of water in the origin of podiform chromitite deposits. *Earth Planet Sci Lett* 203:235–243
- McSkimin HJ, Andreatch P (1972) Elastic moduli of diamonds as a function of pressure and temperature. *J Appl Phys* 43:2944–2945

- Miettinen J (1998) Reassessed thermodynamic solution phase data for ternary Fe-Si-C system. *CALPHAD: Comput Coupling Ph Diagr Thermochem* 22:231–256
- Moody JB (1976) An experimental study on the serpentinization of iron-bearing olivines. *Can Mineral* 14:462–478
- Mookherjee M, Nakajima Y, Steinle-Neumann G, Glazyrin K, Wu XA, Dubrovinsky L, McCammon C, Chumakov A (2011) High-pressure behavior of iron carbide ( $\text{Fe}_7\text{C}_3$ ) at inner core conditions. *J Geophys Res Solid Earth* 116:B04201
- Moore RO, Gurney JJ (1989) Mineral inclusions in diamond from the Monastery kimberlite, South Africa. *Kimberl Relat Rocks* 2:1029–1041
- Moore RO, Otter ML, Rickard RS, Harris JW, Gurney JJ (1986) The occurrence of moissanite and ferro-periclase as inclusions in diamond. In: 4th international kimberlite conference, vol 16. Geological Society of Australia, Perth, pp 409–411
- Müller M, Erhart P, Albe K (2007) Analytic bond-order potential for bcc and fcc iron—comparison with established embedded-atom method potentials. *J Phys Condens Matter*. doi:10.1088/0953-8984/19/32/326220
- Mungall JE, Naldrett AJ (2008) Ore deposits of the platinum-group elements. *Elements* 4:253–258
- Nakajima Y, Takahashi E, Suzuki T, Funakoshi K (2009) “Carbon in the core” revisited. *Phys Earth Planet Inter* 174:202–211
- Nakajima Y, Takahashi E, Sata N, Nishihara Y, Hirose K, Funakoshi K, Ohishi Y (2011) Thermoelastic property and high-pressure stability of  $\text{Fe}_7\text{C}_3$ : implication for iron-carbide in the Earth’s core. *Am Mineral* 96:1158–1165
- Oka Y, Steinke P, Chatterjee ND (1984) Thermodynamic mixing properties of  $\text{Mg}(\text{Al}, \text{Cr})_2\text{O}_4$  spinel crystalline solution at high temperatures and pressures. *Contrib Miner Petrol* 87:196–204
- Onink M, Brakman CM, Tichelaar FD, Mittemeijer EJ, Vanderzwaag S, Root JH, Konyer NB (1993) The lattice-parameters of austenite and ferrite in Fe-C alloys as functions of carbon concentration and temperature. *Scr Metall Mater* 29:1011–1016
- Palme H, O’Neill HSC (2003) Cosmochemical estimates of mantle composition. *Treatise of geochemistry*, vol 2. Elsevier, Amsterdam, pp 1–38
- Peng GY, Lewis J, Lipin B, McGee J, Bao PS, Wang XB (1995) Inclusions of phlogopite and phlogopite hydrates in chromite from the Hongguleng ophiolite in Xinjiang, northwest China. *Am Mineral* 80:1307–1316
- Pineau F, Shilobreeva S, Hekinian R, Bideau D, Javoy M (2004) Deep-sea explosive activity on the Mid-Atlantic Ridge near 34°50' N: a stable isotope (C, H, O) study. *Chem Geol* 211:159–175
- Ponomareva AV, Ruban AV, Vekilova OY, Simak SI, Abrikosov IA (2011) Effect of pressure on phase stability in Fe–Cr alloys. *Phys Rev B Condens Matter Mater Phys* 84:094422
- Poustovetov AA, Roeder PL (2001) The distribution of Cr between basaltic melt and chromian spinel as an oxygen geobarometer. *Can Mineral* 39:309–317
- Ramdohr P (1967) A widespread mineral association connected with serpentinization. *Neues Jahrb Mineral* 107:241–265
- Robinson PT, Bai WJ, Malpas J, Yang JS, Zhou MF, Fang QS, Hu XF, Cameron S, Staudigl H (2004) Ultra-high pressure minerals in the Luobusa ophiolite, Tibet, and their tectonic implications. *Geol Soc Lond Spec Publ* 226:247–271
- Robinson PT, Trumbull RB, Schmitt A, Yang JS, Li JW, Zhou MF, Erzinger J, Dare S, Xiong F (2015) The origin and significance of crustal minerals in ophiolitic chromitites and peridotites. *Gondwana Res* 27:486–506
- Rohrbach A, Schmidt MW (2011) Redox freezing and melting in the Earth’s deep mantle resulting from carbon–iron redox coupling. *Nature* 472:209–212
- Rohrbach A, Ghosh S, Schmidt MW, Wijbrans CH, Klemme S (2014) The stability of Fe–Ni carbides in the Earth’s mantle: evidence for a low Fe–Ni–C melt fraction in the deep mantle. *Earth Planet Sci Lett* 388:211–221
- Salter VJM, Stracke A (2004) Composition of the depleted mantle. *Geochem Geophys Geosyst*. doi:10.1029/2003GC000597
- Schmidt MW, Gao C, Golubkova A, Rohrbach A, Connolly JAD (2014) Natural moissanite (SiC)—a low temperature mineral formed from highly fractionated ultra-reducing COH-fluids. *Prog Earth Planet Sci* 1:27
- Shang SL, Saengdeejing A, Mei ZG, Kim DE, Zhang H, Ganeshan S, Wang Y, Liu ZK (2010) First-principles calculations of pure elements: equations of state and elastic stiffness constants. *Comput Mater Sci* 48:813–826
- Shiryaev AA, Griffin WL, Stoyanov E (2011) Moissanite (SiC) from kimberlites: polytypes, trace elements, inclusions and speculations on origin. *Lithos* 122:152–164
- Shterenberg LE, Slesarev VN, Korsunskaya IA, Kamenetskaya DS (1975) The experimental study of the interaction between the melt carbides and diamond in the iron–carbon system at high pressures. *High Temp High Press* 7:517–522
- Slack GA, Bartram SF (1975) Thermal expansion of some diamond like crystals. *J Appl Phys* 46:89–98
- Sleep NH, Meibom A, Fridriksson T, Coleman RG, Bird DK (2004) H<sub>2</sub>-rich fluids from serpentinization: geochemical and biotic implications. *Proc Natl Acad Sci USA* 101:12818–12823
- Stixrude L, Lithgow-Bertelloni C (2011) Thermodynamics of mantle minerals—II. Phase equilibria. *Geophys J Int* 184:1180–1213
- Trumbull RB, Yang JS, Robinson PT, Di Pierro S, Vennemann T, Wiedenbeck M (2009) The carbon isotope composition of natural SiC (moissanite) from the Earth’s mantle: new discoveries from ophiolites. *Lithos* 113:612–620
- Tsuzuki A, Sago S, Hirano SI, Naka S (1984) High-temperature and pressure preparation and properties of iron carbides  $\text{Fe}_7\text{C}_3$  and  $\text{Fe}_3\text{C}$ . *J Mater Sci* 19:2513–2518
- Ulmer GC, Grandstaff DE, Woermann E, Gobbels M, Schonitz M, Woodland AB (1998) The redox stability of moissanite (SiC) compared with metal-metal oxide buffers at 1773 K and at pressures up to 90 kbar. *Neues Jahrb Mineral* 172:279–307
- Wood IG, Vočadlo L, Knight KS, Dobson DP, Marshall WG, Price GD, Brodholt J (2004) Thermal expansion and crystal structure of cementite,  $\text{Fe}_3\text{C}$ , between 4 and 600 K determined by time-of-flight neutron powder diffraction. *J Appl Crystallogr* 37:82–90
- Xiong W, Hedström P, Selleby M, Odqvist J, Thuvander M, Chen Q (2011) An improved thermodynamic modeling of the Fe–Cr system down to zero kelvin coupled with key experiments. *CALPHAD* 35:355–366
- Xu ST, Wu WP, Xiao WS, Yang JS, Chen J, Ji SY, Liu YC (2008) Moissanite in serpentinite from the Dabie Mountains in China. *Mineral Mag* 72:899–908
- Yamamoto S, Komiya T, Hirose K, Maruyama S (2009) Coesite and clinopyroxene exsolution lamellae in chromites: in-situ ultra-high-pressure evidence from podiform chromitites in the Luobusa ophiolite, southern Tibet. *Lithos* 109:314–322
- Yang JS, Dobrzhinetskaya L, Bai WJ, Fang QS, Robinson PT, Zhang J, Green HW (2007) Diamond- and coesite-bearing chromitites from the Luobusa ophiolite, Tibet. *Geology* 35:875–878
- Zedgenizov DA, Ragozin AL, Shatsky VS, Araujo D, Griffin WL, Kagi H (2009) Mg and Fe-rich carbonate-silicate high-density fluids in cuboid diamonds from the Internationalnaya kimberlite pipe (Yakutia). *Lithos* 112:638–647
- Zhou M-F, Robinson PT, Malpas J, Li Z (1996) Podiform chromitites in the Luobusa ophiolite (Southern Tibet): implications for melt-rock interaction and chromite segregation in the upper mantle. *J Petrol* 37:3–21